Science Advances
AAAS

advances.sciencemag.org/cgi/content/full/5/10/eaax6497/DC1

Supplementary Materials for

Common architecture of Tc toxins from human and insect pathogenic bacteria

F. Leidreiter, D. Roderer, D. Meusch, C. Gatsogiannis, R. Benz, S. Raunser*

*Corresponding author. Email: stefan.raunser@mpi-dortmund.mpg.de

Published 16 October 2019, *Sci. Adv.* **5**, eaax6497 (2019)
DOI: 10.1126/sciadv.aax6497

The PDF file includes:

Other Supplementary Material for this manuscript includes the following:

(available at advances.sciencemag.org/cgi/content/full/5/10/eaax6497/DC1)

Supplementary Figures and Tables

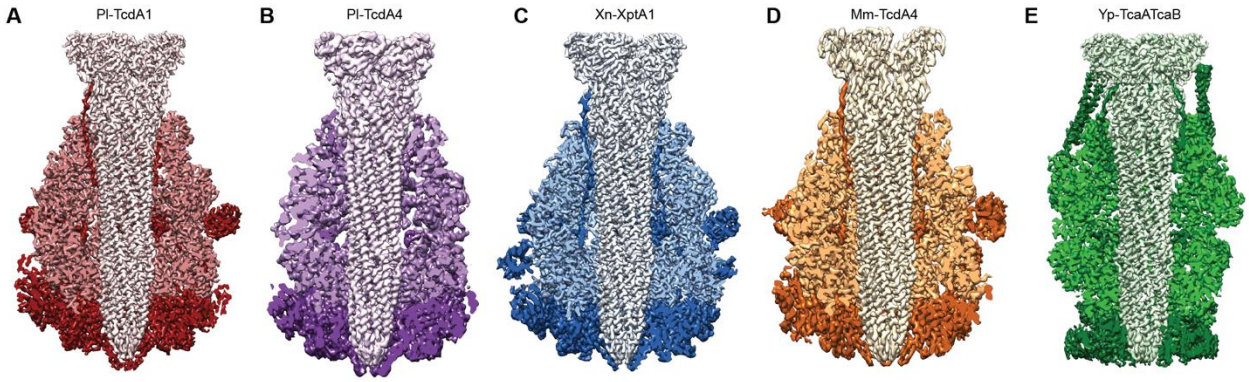

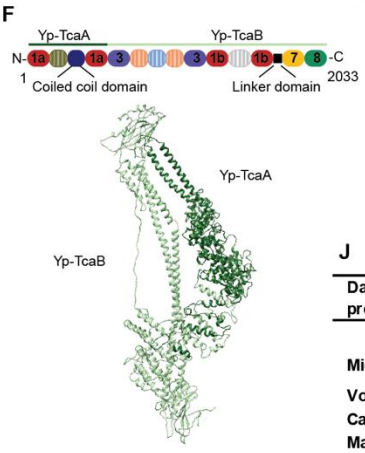

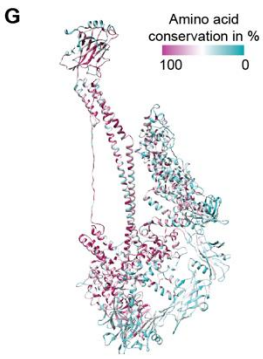

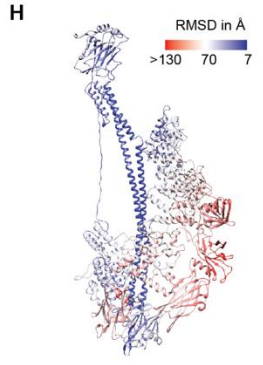

I

Protein	Organism	Holotoxin subunit
Pl-TcdA1	*P. luminescens*	TcA
Pl-TcdA4	*P. luminescens*	TcA
Xn-XptA1	*X. nematophila*	TcA
Mm-TcdA4	*M. morganii*	TcA
Yp-TcaATcaB	*Y. pseudotuberculosis*	TcA

J

Data Collection and processing	Pl-TcdA1	Xn-XptA1	Mm -TcdA4	Pl-TcdA4	Yp-TcaATcaB
Microscope	FEI Titan Krios (Cs corrected, XFEG)				
Voltage (kV)	300				
Camera	FEI Falcon II				FEI Falcon III
Magnification (nominal)	59,000	59,000	59,000	59,000	96,000
Pixel size (Å)	1.14	1.14	1.14	1.12	0.68
Number of frames	25	25	25	7	59
Total electron dose ($e^-/Å^2$)	100	60	60	30.7	130
Exposure time (s)	1.5	1.5	1.5	1	1.5
Defocus range (μm)	0.8 - 2.5	0.7 - 3.0	0.9 - 2.4	1.1 - 3.6	1.0 - 2.2
Number of particles (initial / for final refinement)	634,287 / 436,273	565,210 / 218,992	479,289 / 247,513	35,995 / 35,857	440,777 / 237,295
Map resolution (Å) (FSC threshold)	2.75 (0.143)	2.84 (0.143)	3.27 (0.143)	4.0 (0.143)	3.25 (0.143)
Map sharpening B-Factor ($Å^2$)	-57.91	-52.73	-46.81	-44.32	-111.25
Atomic Model Composition					
Non-Hydrogen atoms	98,645	93,500	88,700	92,095	75,405
Protein residues	12,425	11,685	11,425	11,525	9365
Completeness (%)	98.77	92.63	92.55	96.81	92.13
R.m.s deviations					
Bond lengths (Å)	0.00	0.01	0.01	0.01	0.01
Angles (°)	0.02	1.04	1.06	0.90	0.97
Model Validation					
Clashscore, all atoms	4.09	6.14	5.98	6.17	4.65
Poor rotamers (%)	0.00	0.05	0.32	0.4	0.36
Favored rotamers (%)	98.58	97.84	97.06	97.78	97.62
Ramachandran outliers (%)	0.04	0.26	0.04	0.04	0.00
Ramachandran favored (%)	97.74	92.75	93.27	93.74	90.11
Molprobity score	1.22	1.77	1.74	1.73	1.75

Fig. S1. Structure and conservation of TcAs. (**A-E**) Longitudinal section through the density maps of the five TcAs to display the pore-forming channel. The outer shell encloses the tip of the channel completely in Pl-TcdA1 and Pl-TcdA4, but not in Xn-XptA1, Mm-TcdA4 and Yp-TcaATcaB. Color gradient from light to dark according to Fig. 1. (**F**) Structure of a Yp-TcaATcaB protomer showing the two components Yp-TcaA (light green) and Yp-TcaB (dark green) as well as the domain sequence. (**G**) Structure of a Pl-TcdA1 protomer demonstrating the conservation of residues between Pl-TcdA1, Xn-XptA1, Pl-TcdA4, Mm-TcdA4 and Yp-TcaATcaB. Highly conserved residues are depicted in magenta, less conserved residues are depicted in cyan. (**H**) Structure of a Pl-TcdA1 protomer colored according to the root mean square deviation (RMSD) values between the five TcAs. Regions with high and low RMSDs are depicted in red and blue, respectively. (**I**) Table giving an overview of proteins used in this study. See also Movie S1. (**J**): Cryo-EM data collection and model refinement statistics for all structures.

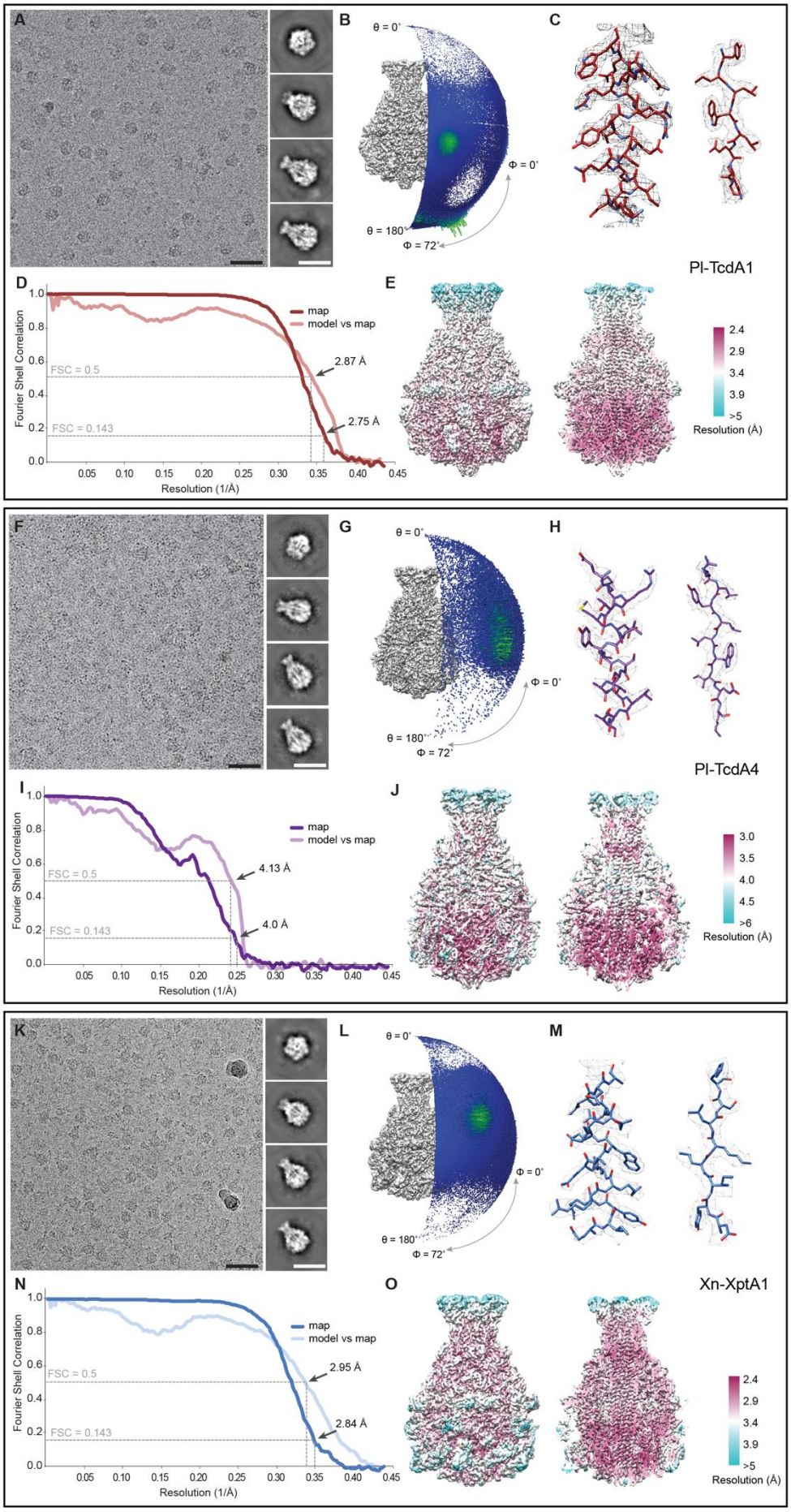
A
B
θ = 0°
Φ = 0°
θ = 180°
Φ = 72°
C
Pl-TcdA1
D
Fourier Shell Correlation
map
model vs map
FSC = 0.5
2.87 Å
FSC = 0.143
2.75 Å
Resolution (1/Å)
E
2.4
2.9
3.4
3.9
>5
Resolution (Å)
F
G
θ = 0°
Φ = 0°
θ = 180°
Φ = 72°
H
Pl-TcdA4
I
Fourier Shell Correlation
map
model vs map
FSC = 0.5
4.13 Å
FSC = 0.143
4.0 Å
Resolution (1/Å)
J
3.0
3.5
4.0
4.5
>6
Resolution (Å)
K
L
θ = 0°
Φ = 0°
θ = 180°
Φ = 72°
M
Xn-XptA1
N
Fourier Shell Correlation
map
model vs map
FSC = 0.5
2.95 Å
FSC = 0.143
2.84 Å
Resolution (1/Å)
O
2.4
2.9
3.4
3.9
>5
Resolution (Å)

Fig. S2. Cryo-EM of Pl-TcdA1, Pl-TcdA4, and Xn-XptA1. (**A**, **F**, **K**) Typical motion-corrected micrographs (scale bars, 50 nm) and 2D class averages (scale bars, 25 nm). (**B**, **G**, **L**) Angular distribution of all particles used for the final reconstruction. (**C**, **H**, **M**) Cryo-EM density (mesh) with the fitted atomic model, showing an α-helical part (left) and a β-strand region (right). (**D**, **I**, **N**) Fourier shell correlation (FSC) curves of the final, filtered density maps. The average resolution at 0.143 FSC criterion is indicated. The light curves shows the FSC curve between the final map versus the atomic model. (**E**, **J**, **O**) EM density maps colored according to the local resolution, showing the complete electron density and a longitudinal section through the density maps.

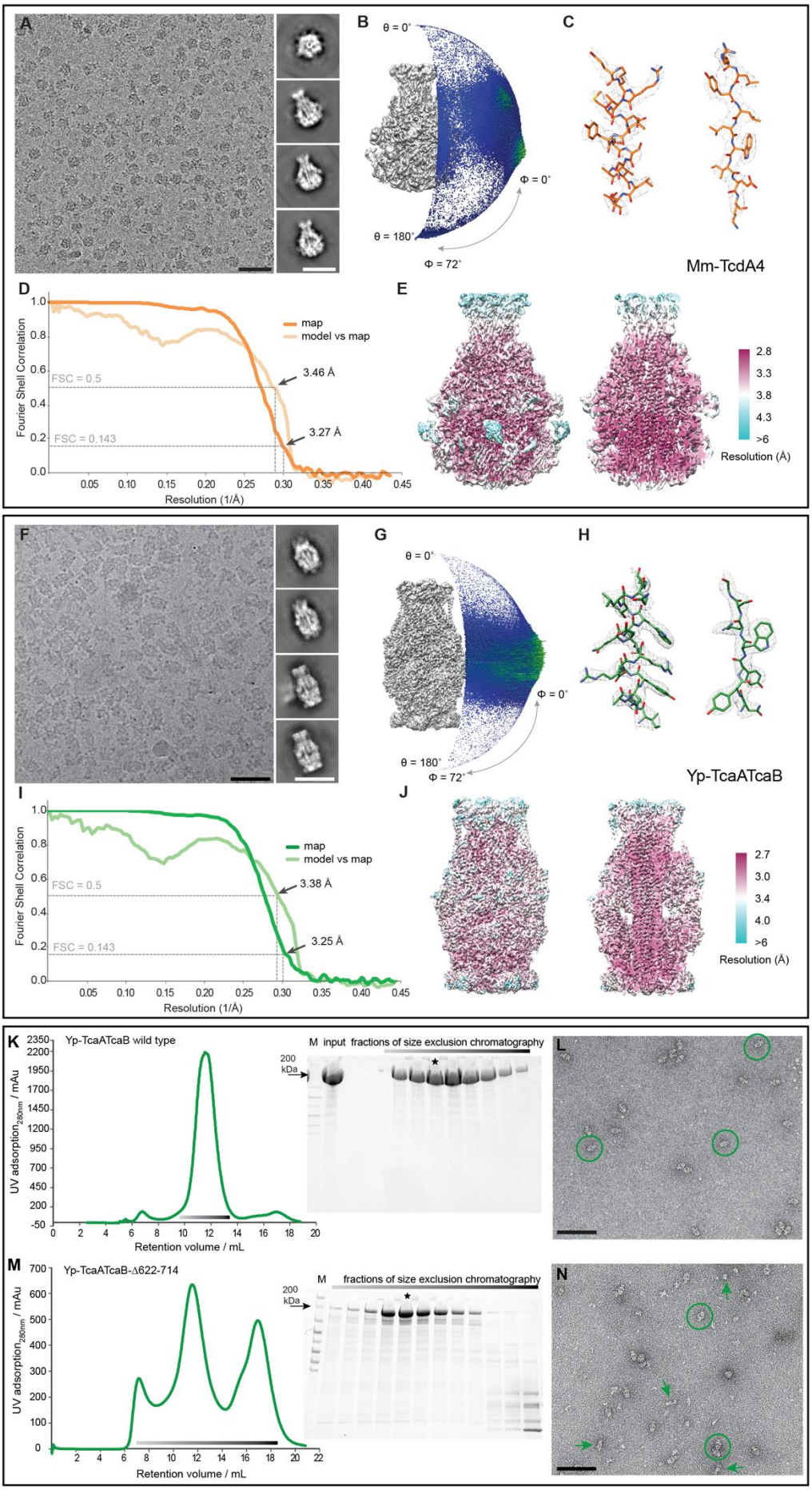
A
B
θ = 0°
Φ = 0°
θ = 180°
Φ = 72°
C
Mm-TcdA4
D
Fourier Shell Correlation
map
model vs map
FSC = 0.5
3.46 Å
FSC = 0.143
3.27 Å
Resolution (1/Å)
E
2.8
3.3
3.8
4.3
>6
Resolution (Å)
F
G
θ = 0°
Φ = 0°
θ = 180°
Φ = 72°
H
Yp-TcaATcaB
I
Fourier Shell Correlation
map
model vs map
FSC = 0.5
3.38 Å
FSC = 0.143
3.25 Å
Resolution (1/Å)
J
2.7
3.0
3.4
4.0
>6
Resolution (Å)
K
Yp-TcaATcaB wild type
UV adsorption280nm / mAu
Retention volume / mL
M input fractions of size exclusion chromatography
200 kDa
L
M
Yp-TcaATcaB-Δ622-714
UV adsorption280nm / mAu
Retention volume / mL
M fractions of size exclusion chromatography
200 kDa
N

Fig. S3. Cryo-EM of Mm-TcdA4 and Yp-TcaATcaB and purification of Yp-TcaATcaB(WT) and Yp-TcaATcaB–Δ622–714. (**A**, **F**) Typical motion-corrected micrographs (scale bars, 50 nm) and 2D class averages (scale bars, 25 nm). (**B**, **G**) Angular distribution of all particles used for the final reconstruction. (**C**, **H**) Cryo-EM density (mesh) with the fitted atomic model, showing an α-helical part (left) and a β-strand region (right). (**D**, **I**) Fourier shell correlation (FSC) curves of the final, filtered density maps. The average resolution at 0.143 FSC criterion is indicated. The light curves shows the FSC curve between the final map versus the atomic model (**E**, **J**) EM density maps colored according to the local resolution, showing the complete electron density and a longitudinal section through the density maps. (**K-N**) Purification of Yp-TcaATcaB (WT) and the mutant Yp-TcaATcaB-Δ622-714. (K, M) Chromatograms of the size exclusion chromatography and corresponding SDS-PAGE gels of Yp-TcaATcaB WT (K**)** and Yp-TcaATcaB-Δ622-714 (M). M=marker and fractions of size exclusion chromatography with increasing retention volume visualized with a gradient from light grey to black. The star marks the band corresponding fraction used for electron microscopy. (L, N) Negative stain electron micrograph of the purified protein Yp-TcaATcaB WT (L) and Yp-TcaATcaB-Δ622-714 (N). Some exemplary particles in the prepore state are marked with solid circles and smaller particles with arrows in (N). Scale bars, 100 nm.

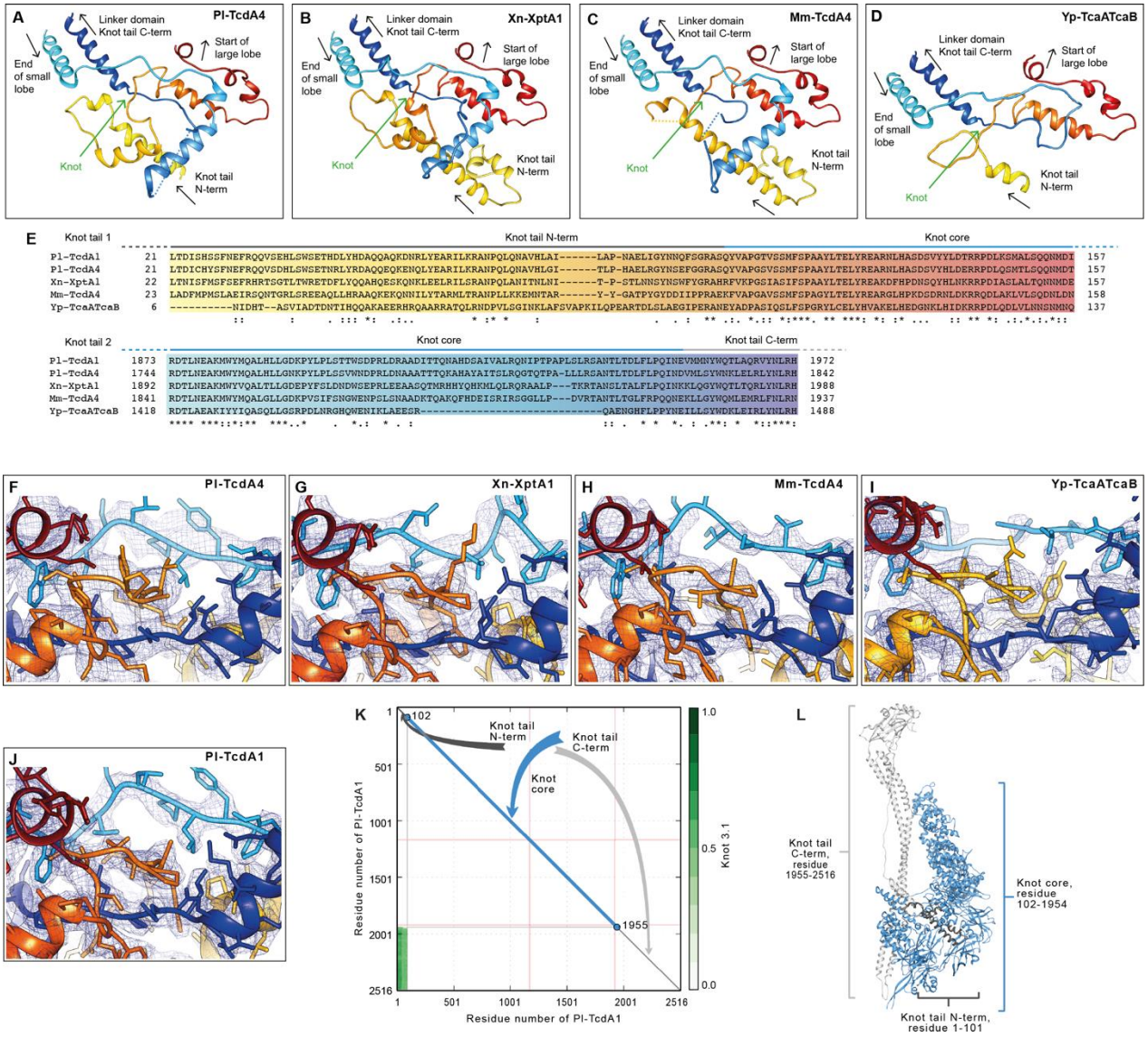

Fig. S4. A 3_1 trefoil protein knot is present in all five TcAs. (**A-D**) Close-up view of the protein knot of Pl-TcdA4 (A), Xn-XptA1 (B), Mm-TcdA4 (C) and Yp-TcaATcaB (D), respectively. The arrows indicate the direction of sequence. The C-terminal knot tail is colored in a red-to-yellow gradient and the N-terminal knot tail is colored in a dark-to-light blue gradient. (**E**) Protein sequence alignment of the two tails of the protein knot. The color gradient is identical to panels A-D and the location of the knot regions are depicted in dark grey, blue and light grey, respectively. (**F-J**) Cryo-EM density maps of the knot region of Pl-TcdA4 (F), Xn-XptA1 (G), Mm-TcdA4 (H), Yp-TcaATcaB (I) and Pl-TcdA1 (J), shown as mesh with each of the aligned atomic structures colored in rainbow gradients. (**K**) Matrix scheme of the 3_1 trefoil

protein knot with the three domains of the knot organization: knot tail N terminus (dark grey), the knot core (blue) and the knot tail C terminus (grey). Residues that belong to the knot tails are colored in green in the matrix. The intensity of the green color gradient on the right represents the probability of detecting a 3_1 trefoil knot ranging from no probability (white) to high probability (dark green). (**L**) Structure of a Pl-TcdA1 protomer colored according to the three different knot domains. See also Movie S2.

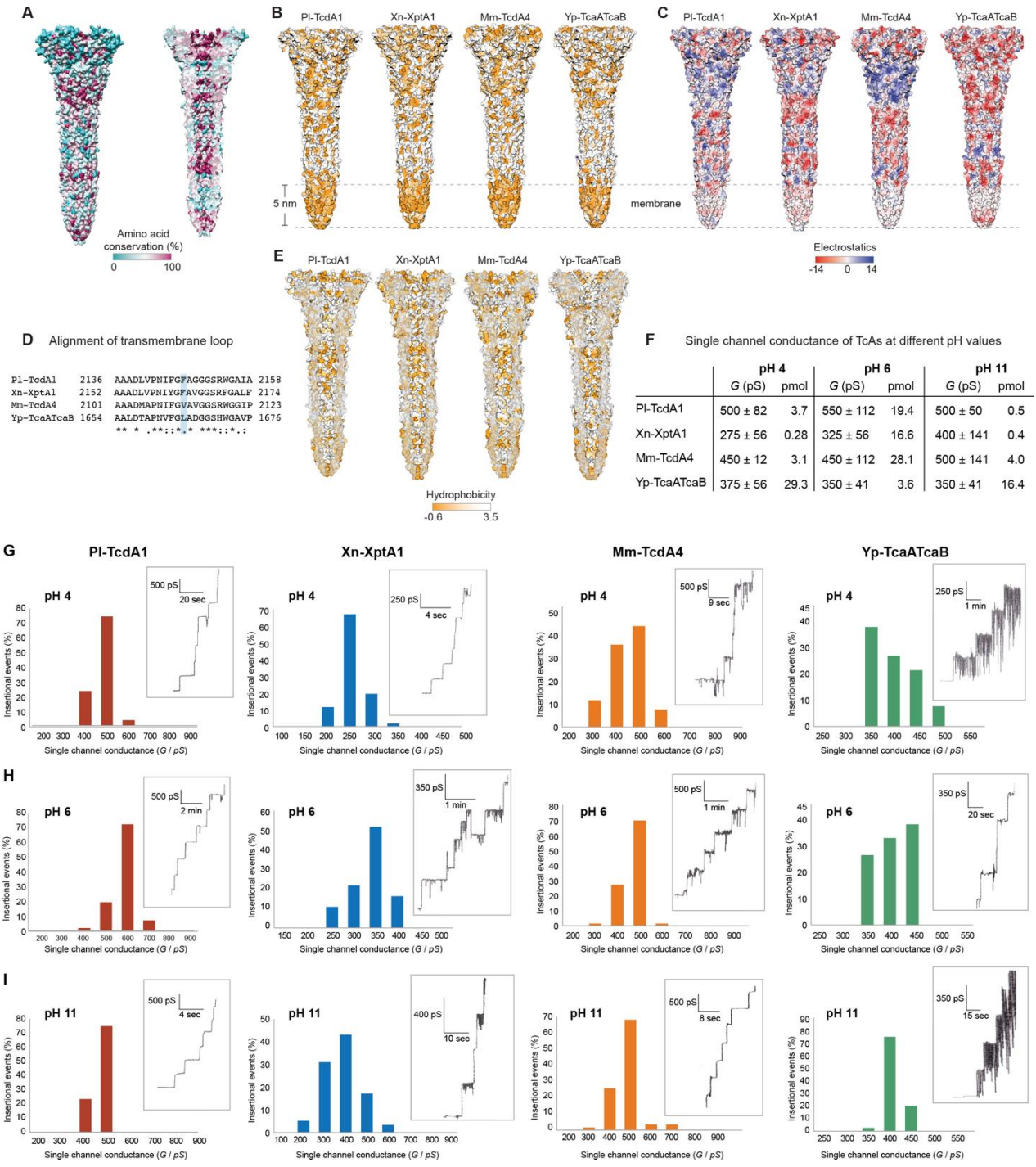

Fig. S5. Biophysical properties of the TcA channels. (**A**) Residue conservation plot of the channel domains of the four TcAs, shown for the channel surface (left) and the lumen of the channel (right). Conserved residues are shown in magenta. (**B**) Surface representation of the channels of Pl-TcdA1, Xn-XptA1, Mm-TcdA4 and Yp-TcaATcaB, colored by hydrophobicity. (**C**) Surface representation of the channels, colored by the Coulomb potential at pH 7. Positively

charged (14 kcal/mol) and negatively charged (-14 kcal/mol) residues are colored in blue and red, respectively. (**D**) Sequence alignment of the transmembrane loop of the channel domains. The residue at the very tip of the channel domain is highlighted in light blue. (**E**) Cross-sections of the channels, showing the hydrophobicity at the channel inner surface. (**F**) Table listing the average single channel conductivity obtained from black lipid bilayer experiments and the amount of TcA used for each experiment to obtain at least 70 pores. (**G-I**) Measurements of Pl-TcdA1, Xn-XptA1, Mm-TcdA4 and Yp-TcaATcaB were performed at pH 4, 6 and 11, respectively. For each experiment, an exemplary recording of the single channel current versus time is attached. All histograms were constructed from the data of at least 70 pore insertional events for each TcA and pH value.

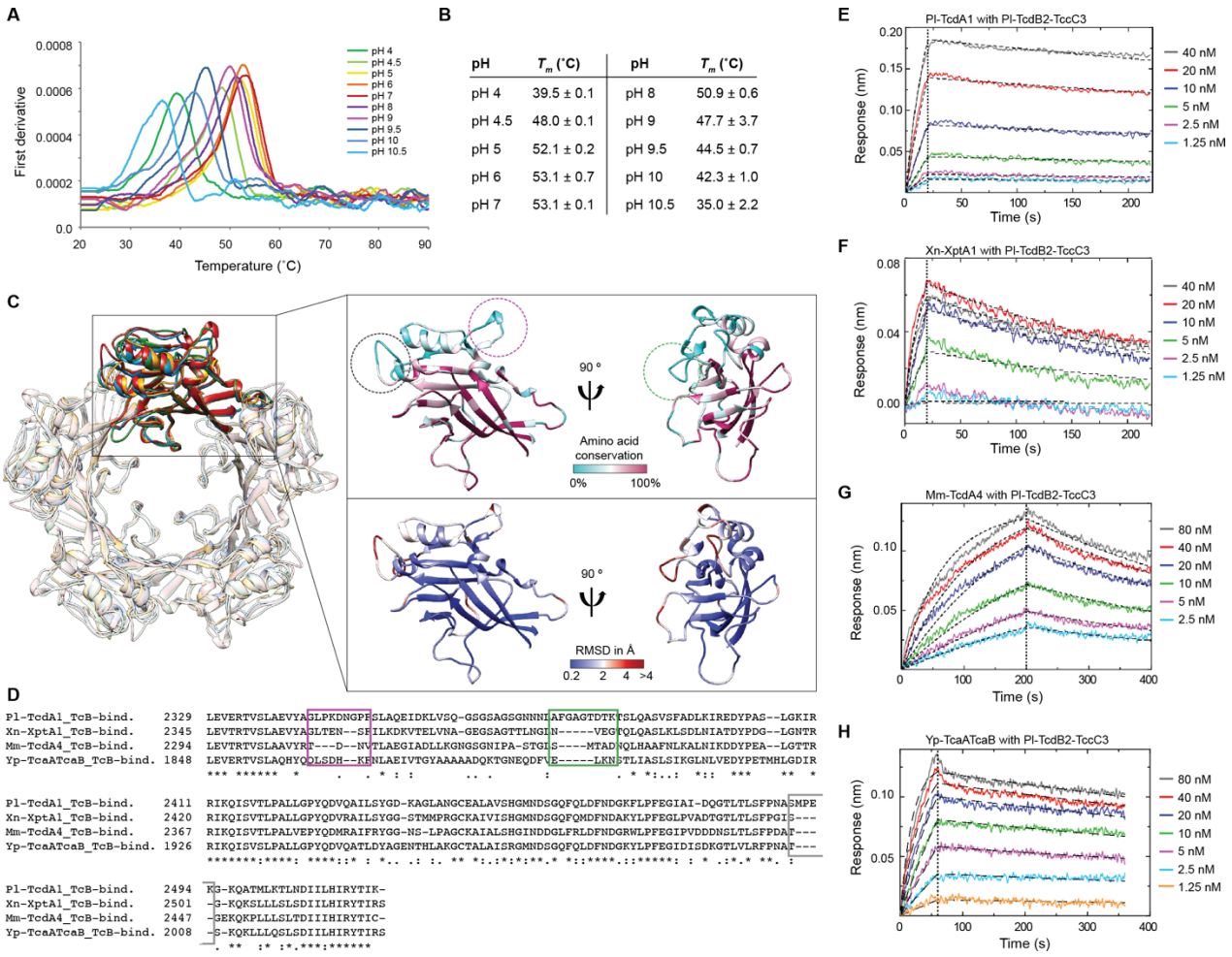

Fig. S6. pH stability of Yp-TcaATcaB and characterization of chimeric holotoxin formation. (**A**, **B**) Nano differential scanning fluorimetry of Yp-TcaATcaB at different pH values. (A) The graph shows the first derivate of the absorbance quotient (330 nm/350 nm) as function of temperature. The different pH values are indicated by different colors. (B) Table with the melting temperatures (T_m) for each pH value. The measurements were performed in triplicates and the T_m is given as the mean ± standard deviation. (**C**) Comparison of the TcB-binding domains. Left panel shows an overlay of the pentameric TcB-binding domains of Pl-TcdA1, Xn-XptA1, Mm-TcdA4 and Yp-TcaATcaB colored in red, blue, orange and green, respectively. One protomer is highlighted. The right panel shows TcB-binding domain of one protomer of Pl-TcdA1 demonstrating the conservation (upper panel) of residues between Pl-TcdA1, Xn-XptA1, Mm-TcdA4 and Yp-TcaATcaB and the RMSD of the TcB-binding domain

structures (lower panel). Conserved residues are depicted in magenta. The three non-conserved loops are highlighted with dashed circles and the respective sequences are highlighted in (**D**). Residues with a low RMSD are colored in blue. (D) Sequence alignment of the TcB-binding domain. The loops marked in (C) are indicated in the alignment. (**E-H**) BLI sensorgrams of Pl-TcdA1 (E), Xn-XptA1 (F) Mm-TcdA4 (G) and Yp-TcaATcaB (H) interacting with immobilized Pl- TcdB2-TccC3. TcA pentamer concentrations were 1.25 - 40 nM in (E) and (F), 2.5 – 80 nM in (G) and 1.25 - 80 nM in (H). A global fit according to a 1:1 binding model was applied (black dashed curves). Association and dissociation phases are separated by a black dashed line. The obtained K_D, k_{on} and k_{off} values are shown in Fig. 5E.

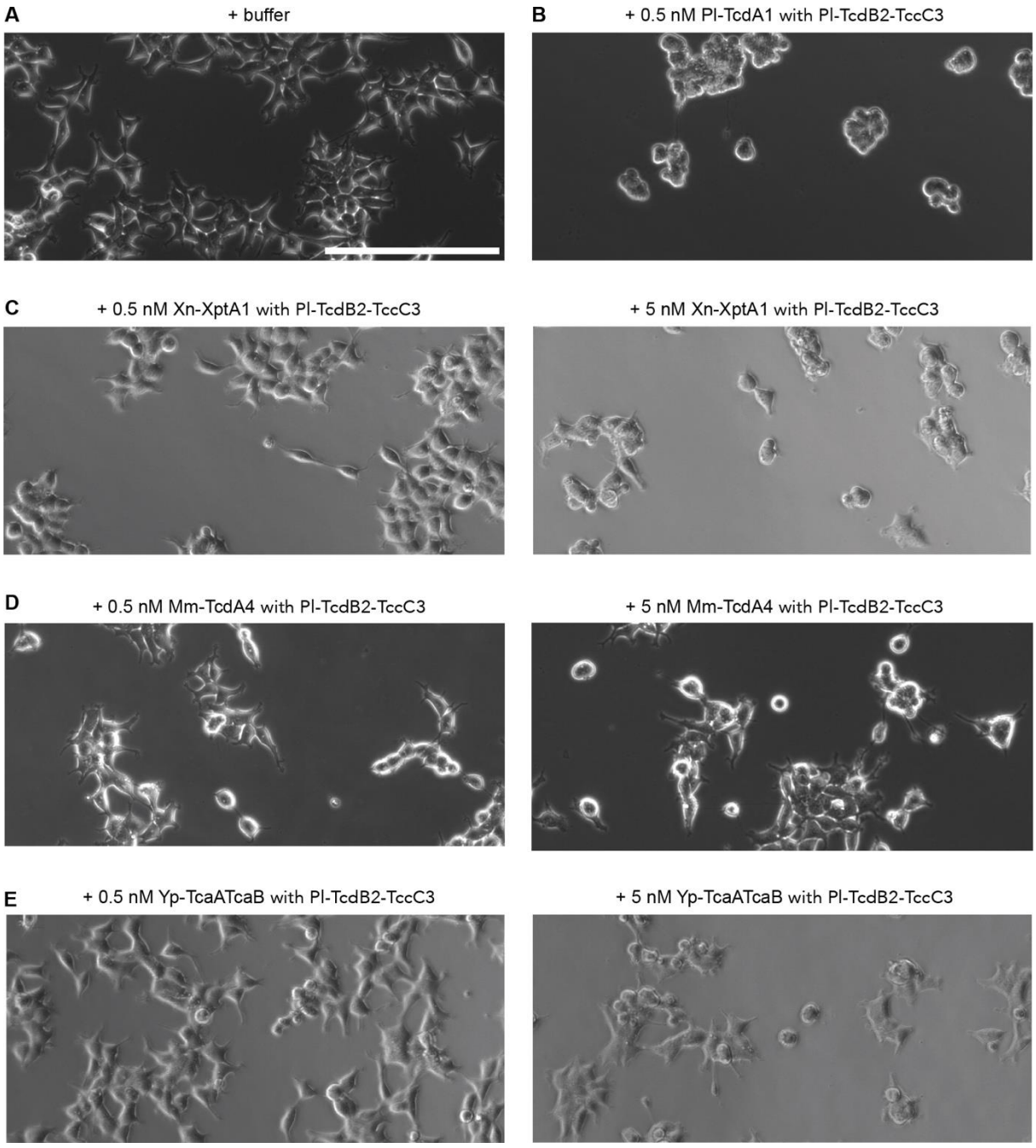

Fig. S7. Intoxication of HEK293T cells with chimeric holotoxins. (**A**) Negative control with only buffer added. (**B**) Positive control with the native holotoxin complex from *P. luminescens* (Pl-TcdA1 and TcdB2-TccC3) at a concentration of 0.5 nM holotoxin. (**C-E**) Effect of the holotoxin complex composed of Pl-TcdB2-TccC3 and Xn-XptA1 (C), or Mm-TcdA4 (D), or Yp-TcaATcaB (E) at concentrations of 0.5 nM (left) and 5 nM (right). Cells were imaged 20 hours after intoxication. Scale bar, 200 µm.

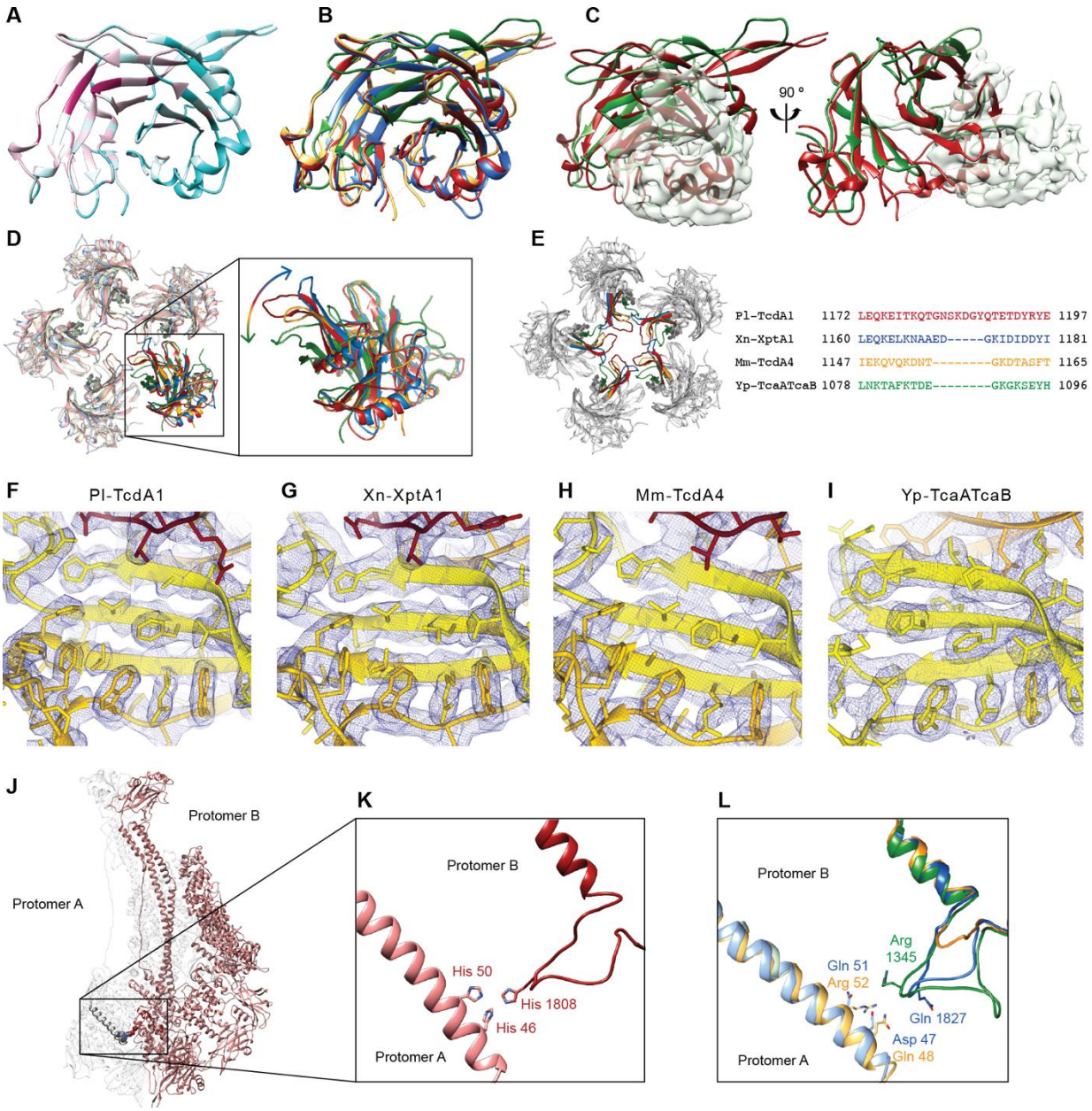

Fig. S8. Topology of neuraminidase-like domain and nonconserved cluster of three histidine residues. (**A**) Conservation of the neuraminidase-like domain with highly conserved regions in magenta and low conservation in turquoise shown for the neuraminidase-like domain of Pl-TcdA1. (**B**) Structural alignment of the neuraminidase-like domain for Pl-TcdA1 (red), Xn-XptA1 (blue), Mm-TcdA4 (yellow) and Yp-TcaATcaB (green). (**C**) Structural alignment of the neuraminidase-like domain of Pl-TcdA1 and Yp-TcaATcaB shown in front (left) and side view (right). To visualize the missing 125 residues of Yp-TcaATcaB, the density map corresponding

to these residues is shown. (**D**) Pentamer of the neuraminidase-like domain of Pl-TcdA1 (red), Xn-XptA1 (blue), Mm-TcdA4 (yellow) and Yp-TcaATcaB (green) with one protomer highlighted and zoomed in. The arrow indicates the different orientation of the loop at the center of the pentamer. (**E**) Pentamer of the neuraminidase-like domain, highlighting the loop and a sequence alignment showing the different lengths of the loop region in respective colors. (**F**-**I**) Cryo-EM density maps of a section of the neuraminidase-like domain of Pl-TcdA1 (F), Xn-XptA1 (G), Mm-TcdA4 (H) and Yp-TcaATcaB (I) shown as mesh with the respective aligned atomic model colored in a rainbow gradient. (**J**-**L**) Non-conserved cluster of three histidine residues in Pl-TcdA1. (J) Two protomers of Pl-TcdA1 indicating the histidine interaction site between two protomers of Pl-TcdA1. (K) A close-up view of the three interacting histidines of Pl-TcdA1. (L) The histidine residues are not conserved in Xn-XptA1 (blue), Mm-TcdA4 (yellow) and Yp-TcaATcaB (green).

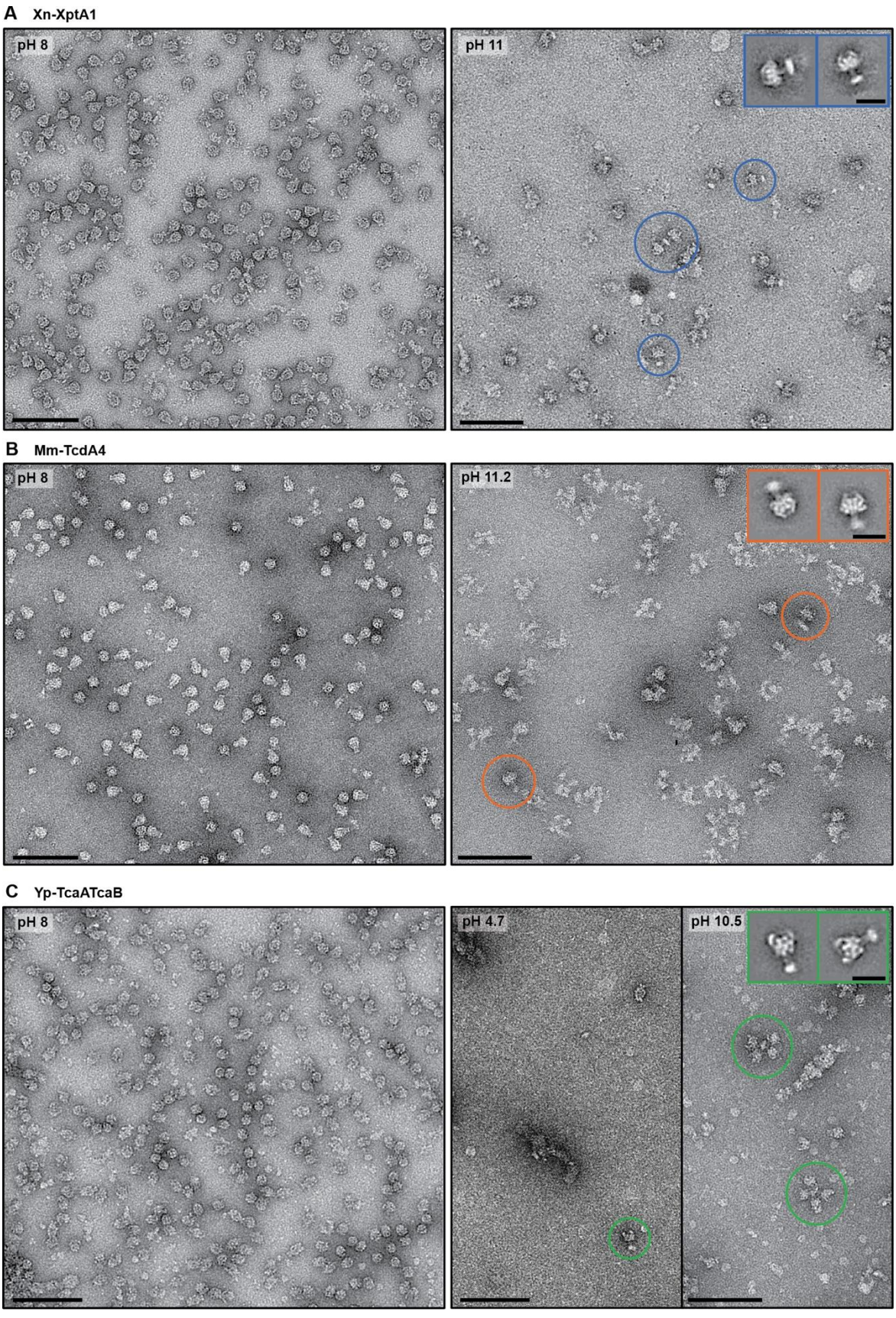
A
Xn-XptA1
pH 8
pH 11
B
Mm-TcdA4
pH 8
pH 11.2
C
Yp-TcaATcaB
pH 8
pH 4.7
pH 10.5

Fig. S9. pH-induced pore formation of Xn-XptA1, Mm-TcdA4, and Yp-TcaATcaB. (**A**) Negative stain electron micrograph of the Xn-XptA1 prepore at pH 8 (left) and the pore reconstituted in nanodiscs at pH 11 in the presence of 3 mM $CaCl_2$ (right). (**B**) Negative stain electron micrographs of the Mm-TcdA4 prepore at pH 8 (left) and the pore reconstituted in nanodiscs at pH 11.2 in the presence of 5 mM $CaCl_2$ (right). (**C**) Negative stain electron micrographs of the Yp-TcaATcaB prepore at pH 8 (left) and the pore reconstituted in nanodiscs at pH 4.7 or pH 10.5 (right). Particles in the pore state are highlighted with colored circles. Scale bars, 100 nm. Insets: Two representative 2D class averages of the pore state of every toxin. Scale bars in the insets, 20 nm.

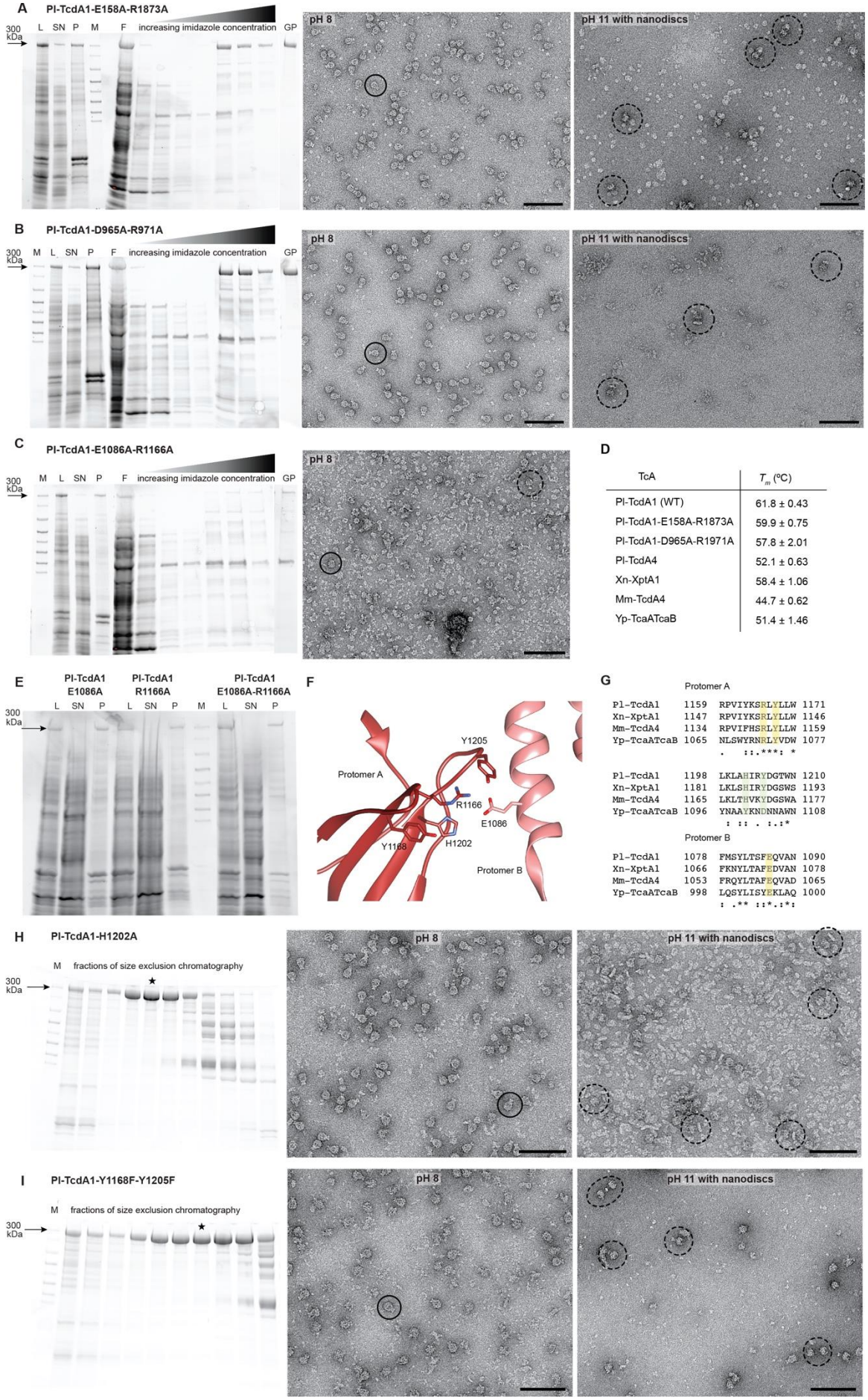
A
Pl-TcdA1-E158A-R1873A
300 kDa
L SN P M F increasing imidazole concentration GP
pH 8
pH 11 with nanodiscs
B
Pl-TcdA1-D965A-R971A
300 kDa
M L SN P F increasing imidazole concentration GP
pH 8
pH 11 with nanodiscs
C
Pl-TcdA1-E1086A-R1166A
300 kDa
M L SN P F increasing imidazole concentration GP
pH 8
D
TcA | T_m (ºC)
Pl-TcdA1 (WT) | 61.8 ± 0.43
Pl-TcdA1-E158A-R1873A | 59.9 ± 0.75
Pl-TcdA1-D965A-R1971A | 57.8 ± 2.01
Pl-TcdA4 | 52.1 ± 0.63
Xn-XptA1 | 58.4 ± 1.06
Mm-TcdA4 | 44.7 ± 0.62
Yp-TcaATcaB | 51.4 ± 1.46
E
Pl-TcdA1 E1086A
Pl-TcdA1 R1166A
Pl-TcdA1 E1086A-R1166A
L SN P L SN P M L SN P
300 kDa
F
Y1205
Protomer A
R1166
E1086
H1202
Y1168
Protomer B
G
Protomer A
Pl-TcdA1 1159 RPVIYKSRLYLLW 1171
Xn-XptA1 1147 RPVIYKSRLYLLW 1146
Mm-TcdA4 1134 RPVIPHSRLYLLW 1159
Yp-TcaATcaB 1065 NLSWYRNRLYVDW 1077
Pl-TcdA1 1198 LKLAHIRYDGTWN 1210
Xn-XptA1 1181 LKLSHIRYDGSWS 1193
Mm-TcdA4 1165 LKLTHVKYDGSWA 1177
Yp-TcaATcaB 1096 YNAAYKNDNNAWN 1108
Protomer B
Pl-TcdA1 1078 FMSYLTSFEQVAN 1090
Xn-XptA1 1066 FKNYLTAFEDVAN 1078
Mm-TcdA4 1053 FRQYLTAFEQVAD 1065
Yp-TcaATcaB 998 LQSYLISYEKLAQ 1000
H
Pl-TcdA1-H1202A
M fractions of size exclusion chromatography
300 kDa
pH 8
pH 11 with nanodiscs
I
Pl-TcdA1-Y1168F-Y1205F
M fractions of size exclusion chromatography
300 kDa
pH 8
pH 11 with nanodiscs

Fig. S10. Mutational studies of Pl-TcdA1. (**A**-**C**) The left panels show SDS-PAGE gels after Ni-NTA purification and gel filtration at pH 8 of Pl-TcdA1-D158A-R1873A (A), Pl-TcdA1D965A and R1971A (B), and Pl-TcdA1-D1086A-R1166A (C). M = marker, L = lysate, SN = supernatant, P = pellet, elutions at increasing imidazole concentrations (5 – 150 mM), GP = gel filtration peak fraction. The 300 kDa band corresponding to the TcA monomer is marked with an arrow. The right panels show negative stain electron micrographs of the peak fraction applied to the grid directly after purification at pH 8 or after reconstitution in nanodiscs at pH 11. Particles in the prepore and pore state are marked with solid and dashed circles, respectively. Due to the insufficient purity of the Pl-TcdA1-E1086A-R1166A variant, the reconstitution step was omitted. (**D**) Table with measured melting temperatures T_m (nanoDSF) for all analyzed TcAs at pH 8. The measurements were performed as triplicates and the mean T_m as well as the standard deviations are shown. (**E**) SDS-PAGE gel after expression of Pl-TcdA1 mutants Pl-TcdA1-E1086A, Pl-TcdA1-R1166A, and Pl-TcdA1-E1086A-R1166A. For all proteins, a sample of the lysate (L), supernatant (SN) and pellet after ultracentrifugation (P) was applied. M = marker. (**F**, **G**) Close-up view of a conserved interaction site in Pl-TcdA1 (F) and alignment of residues, which are involved in the interaction (G). The conserved residues in all four TcAs are highlighted in yellow and the ones only conserved in Pl-TcdA1, Xn-XptA1 and Mm-TcdA4 in green. (**H**, **I**) SDS-PAGE gels of gel filtration fractions (left) of Pl-TcdA1-H1202A (H) and Pl-TcdA1-Y1168F-Y1205F (I) as well as negatively stained complexes at pH 8 (middle) and pH 11 after reconstitution in nanodiscs (right). The toxin-nanodisc ratio was 1:10 in (H), leading to a background of empty nanodiscs. The star marks the band corresponding fraction used for electron microscopy. Particles in the prepore and pore state are marked with solid and dashed circles, respectively. Scale bars, 100 nm.

Movie S1. Cryo-EM density maps of Pl-TcdA1, Pl-TcdA4, Xn-XptA1, Mm-TcdA4, and Yp-TcaATcaB. The EM-density maps are colored in a gradient from light to dark representing the pore domain with the TcB-binding domain, the α-helical shell, the β-sheet domains and the linker. The molecular model is shown for each TcAs and superimposed with the respective cryo-EM density. The colors correspond to those in Fig. 1.

Movie S2. Molecular trefoil knot in Pl-TcdA1. Pl-TcdA1 protomer with the molecular 3_1 trefoil knot highlighted in rainbow colors corresponding to Fig. 3. An alignment of the molecular knot structure of Pl-TcdA1 (red), Xn-XptA1 (blue), Mm-TcdA4 (yellow) and Yp-TcaATcaB (green) show the structural conservation of this region.